

Mineral chemistry, geochemistry, Raman spectroscopy and geotectonic significance of Neoproterozoic ophiolitic peridotites and pyroxenites from Kab Amiri district, central Eastern Desert, Egypt

Sherif Kharbish^{1,*}, Omar Amer², Amr El-Awady²

¹Geology Department, Faculty of Science, Suez University, Suez Governorate, El Salam City, 43518, Egypt

²Geology Department, Faculty of Science, Zagazig University, Zagazig 44519, Egypt

ARTICLE INFO

Article history:

Received 9 November 2019

Received in revised form 24 January 2020

Accepted 24 January 2020

Available online 25 January 2020

Keywords

Neoproterozoic;

ophiolites;

forearc;

Raman spectroscopy;

Egypt;

ABSTRACT

The small gold mining Kab Amiri district ultramafic ophiolitic section (central Eastern Desert) comprises highly serpentinized peridotites (serpentinites) and few pyroxenites. It lies within a region of Neoproterozoic ophiolitic rocks and associated derivatives. The chromian spinel textural and chemical compositional features suggest transitional greenschist-amphibolite up to lower amphibolite facies metamorphism and indicates that they represent highly-depleted mantle residues. The presence of the Si-O_b-Si antisymmetric $\nu_1(A_1)$, symmetric $\nu_2(A_1)$ bands and the hydroxyl group (OH) modes are conclusive for the discrimination of antigorite. Furthermore, the speculation of serpentines as antigorite can also be indicated from the hydroxyl group modes. The Kab Amiri ophiolite suite (central Eastern Desert) represents fragments of oceanic lithosphere that are developed in forearc setting in a supra-subduction zone (SSZ) environment. Thus the low TiO₂ contents, the enrichment in LILE and LREE and the Nb depletion reflect the remelting of a highly depleted mantle source and suggest their formation in a SSZ environment (i.e forearc).

1. Introduction

During the Pan-African Orogen (PAO; 550–900 Ma; Stern, 2004); the Arabian-Nubian Shield (ANS; 690 to 890 Ma, Stern, 2004) was formed, comprising the Neoproterozoic ophiolites (870 to 690 Ma; Stern et al., 2004) in the Eastern Desert (ED) of Egypt. Many authors discussed the Egyptian Neoproterozoic ophiolites (ENO) (e.g. Farahat et al., 2004; Stern et al., 2004; Ali-Bik et al., 2012). Some workers considered the ENO to be generated in mid-ocean ridges (e.g. Zimmer et al. 1995), others thought that they were formed in a forearc (e.g. Stern et al. 2004; Azer and Stern 2007; Khalil and Azer 2007) or in a back-arc setting (e.g. Farahat et al. 2004).

The Kab Amiri district (KAD), central Eastern Desert (CED), Egypt, was long known as a small gold mining district since ancient times (Andráš and Kharbish, 2014). Gold mining in the KAD area dates back to New ancient Egyptian (Pharaonic) dynastic Kingdoms (2700 to 1070 BC) (Kharbish and Andráš 2014a, b). Recently, the KAD area (especially the Kab Amiri granite pluton) is considered as one of the most important U mineralization zones in the CED (Gaafar and Aboelkhair, 2014).

Despite the work that has been done on the different rock units in the KAD, no or rare (to best of my knowledge) detailed studies on the Neoproterozoic ophiolitic rocks in the KAD area, were performed. Thence, the present work aims to establish the primary petrography, bulk-rock and mineral chemistry of Neoproterozoic ophiolitic rocks in the KAD area. This study uncovered a good model for the sophisticated geologic processes experienced by the Egyptian Neoproterozoic ophiolitic rocks, notwithstanding the tricky task of eliciting information from these complex rocks. The serpentine and the spinal minerals were investigated in detail by using the μ -Raman spectroscopic technique. The Raman spectroscopy provides information on structure and composition of many mineralogical groups (e.g. Kharbish 2017) and gives an accurate, obvious identification of major rock-forming minerals (e.g., silicates; Wang et al., 1999), accessory minerals (e.g., phosphates, oxides, and sulfides; Kharbish 2012; Kharbish et al. 2014, Kuebler et al. 2002), and secondary minerals produced by weathering and / or hydrothermal solutions (e.g., sulfates, carbonates, sulfosalts and phyllosilicate clay minerals; Wang et al., 2002; Kuebler et al. 2001; Kharbish et al. 2007, 2009, Kharbish and Andráš, 2014c; Kharbish and Jeleň, 2016; Kharbish 2007, 2011, 2016). It can also distinguish OH and bound and unbound forms of H₂O (Wang et al. 2001).

* Corresponding authors at: Suez University
E-mail addresses: sherif.abdalla@suezuniv.edu.eg;
sherifkharbish@hotmail.com (Sherif Kharbish)

2. Geology and petrography

The KAD area is ~ 45 km far from Port Quseir in the CED of Egypt and lies within a region (from oldest to youngest, Fig. 1) of Neoproterozoic ophiolitic rocks and associated derivatives that are emplaced in island arc, calc-alkaline volcano-sedimentary associations (Fig. 2a) and metagabbro-diorite assemblages (older gabbros), which together with the ophiolitic suites were later intruded by older granitoids and younger granites (Moghazi, 2002). The KAD is dissected by several major faults (Fig. 1), which extend predominantly in NW direction, with a smaller number of faults trending in the NE and E-W directions (Moghazi, 2002; Gaafar and Aboelkhair, 2014). The area has suffered multiple deformation and metamorphism caused by complex tectonic movements during the PAO, where the rocks were deformed and metamorphosed in the greenschist and amphibolite facies (Moghazi, 2002).

The KAD Neoproterozoic ultramafic ophiolitic rocks form an elongated ridge, striking roughly E–W (ENE–WSW) with an average width of about 400 m and extend ~ 8 km eastward as a discontinuous chain (Fig. 1). The extensively serpentinized peridotites (henceforward serpentinites) occupy a large area and are highly deformed and sheared.

The KAD serpentinites (highly serpentinized peridotites) display a massive fine- to medium-grained appearance and grayish to greenish colors.

Petrographically, serpentinites compose basically of fine- to medium-grained platy shreds and fibrous flakes antigorite, together with primary chromian spinel and few amounts of secondary metamorphic minerals talc and chlorite. The rocks commonly preserve pseudomorphic textures of serpentine after orthopyroxene (bastite texture) that testify their harzburgite parentage. Subhedral shape spinel crystals (altered along fractures and grain boundaries) exhibit three irregular optical zoning owing to their alteration processes. The primary chromian spinel (dark gray color under Scan Electron Microscope, SEM) are rimmed or mantled by the intermediate gray zone corresponds to ferrian chromite and the outermost light gray rim of Cr-magnetite (Figs. 2b, c). Rarely chlorite grains occur as small aggregates in a serpentine matrix or as aureoles around altered chromian spinel as well as coating the bastite textures, indicating the chlorite formation by serpentinization.

Pockets or small elongated massive remnants are recorded within the serpentinites that consist mainly of pyroxenites (Fig. 2d). The pyroxenites are predominantly composed of clinopyroxene (diopside + rare augit) and orthopyroxene (enstatite), with antigorite and subordinate amounts of metamorphic minerals (viz., tremolite, talc and chlorite).

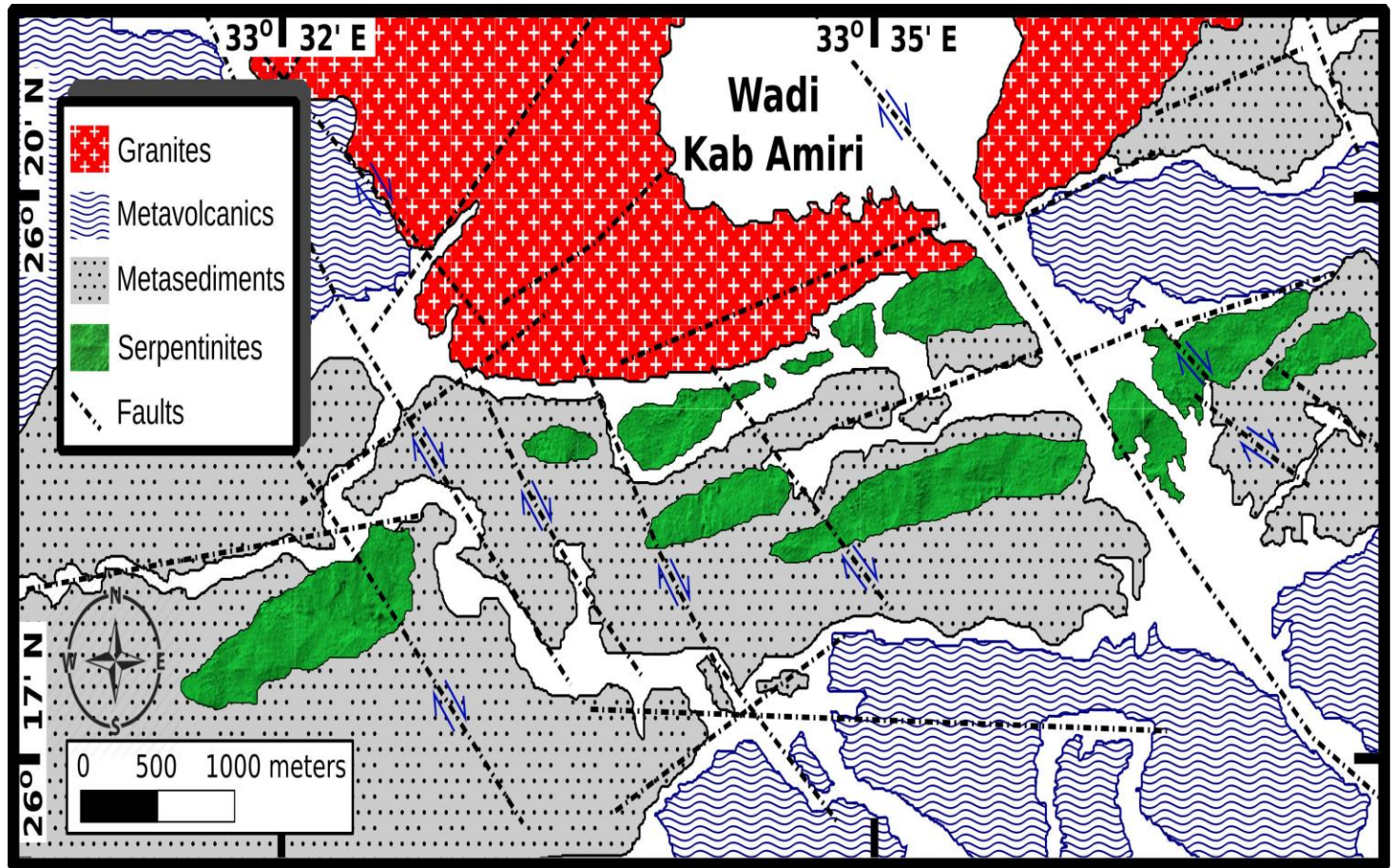


Fig. 1. Geological map of Kab Amiri district, central Eastern Desert, Egypt (modified after Gaafar and Aboelkhair, 2014).

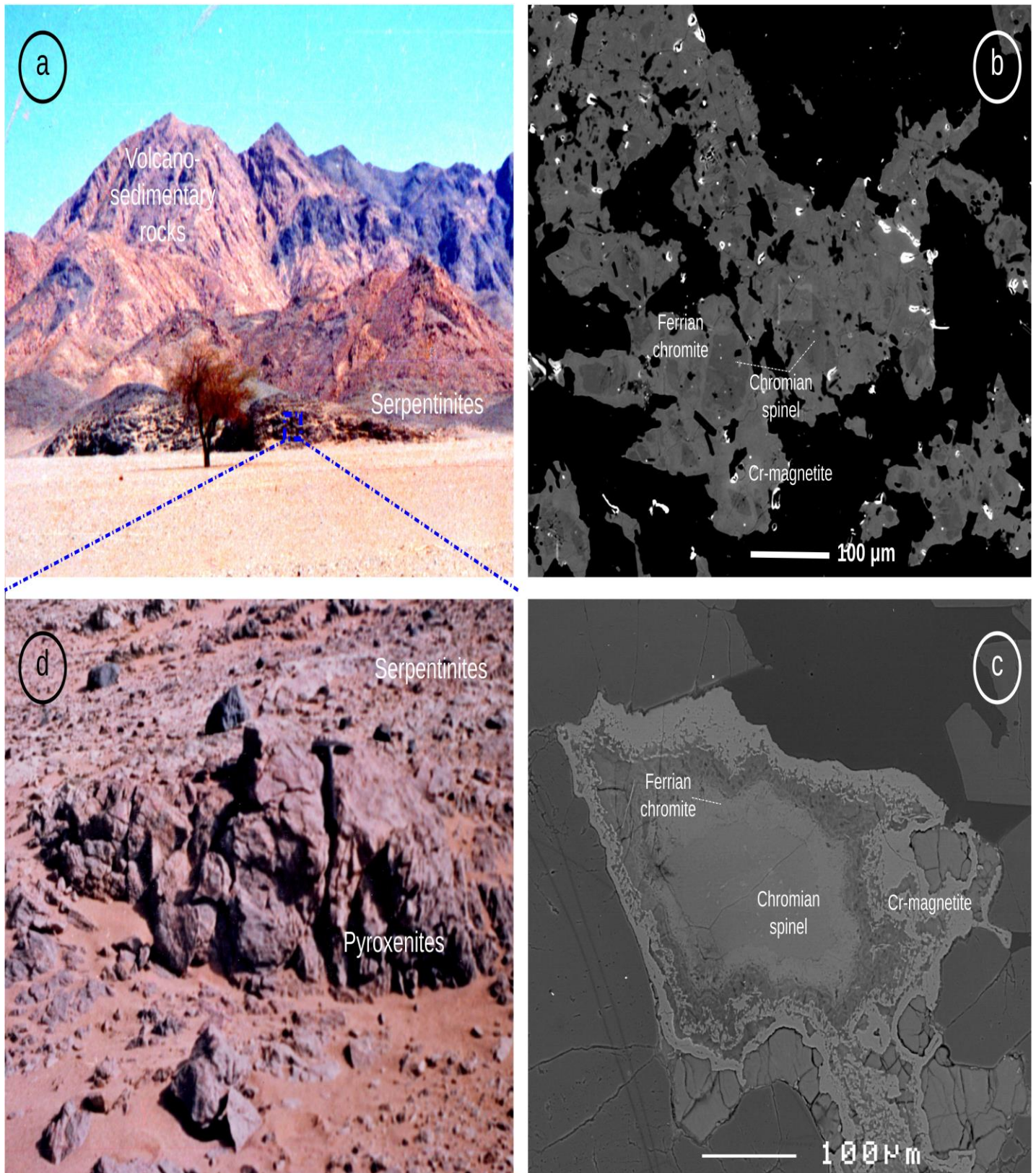


Fig. 2. (a) Contact between the serpentinites and the underlying volcano-sedimentary rocks, (b) pyroxenites in serpentinites, (c) and (d) BE-SEM images illustrating typical zoning patterns of the primary chromian spinel and the metamorphic ferrian chromite and of Cr-magnetite.

3. Samples and experiments

Minerals compositions were obtained by the Cameca microbeam electron microprobe analyzer (EMPA; Cameca SX 100), with 15 Kv accelerating voltage, 20 nA beam current, 1 μm beam diameter and a counting time of 10s. The data were corrected using the ZAF software and calibrated by natural and synthetic reference materials: adularia (Si, Al, K), chromite (Cr, Fe), periclase (Mg), rhodonite (Mn), wollastonite (Ca), pentlandite (Ni), jadeite (Na) and rutile (Ti).

Representative 20 samples (10 serpentinites and 10 pyroxenites) from the KAD area have been analyzed for their major, trace and rare-earth elements (REE) compositions. Bulk rock major and trace elements analyses were performed by the X-ray spectrometer Phillips PW 2400. Analytical precision was better than 1% and 3% for major and trace elements, respectively. The inductively coupled plasma-mass spectrometer (ICP-MS) Elan 6100 with Hg Flow Injection System "FIMS 100" and Laser Sampler "LSX 200" were used for the REE analyses.

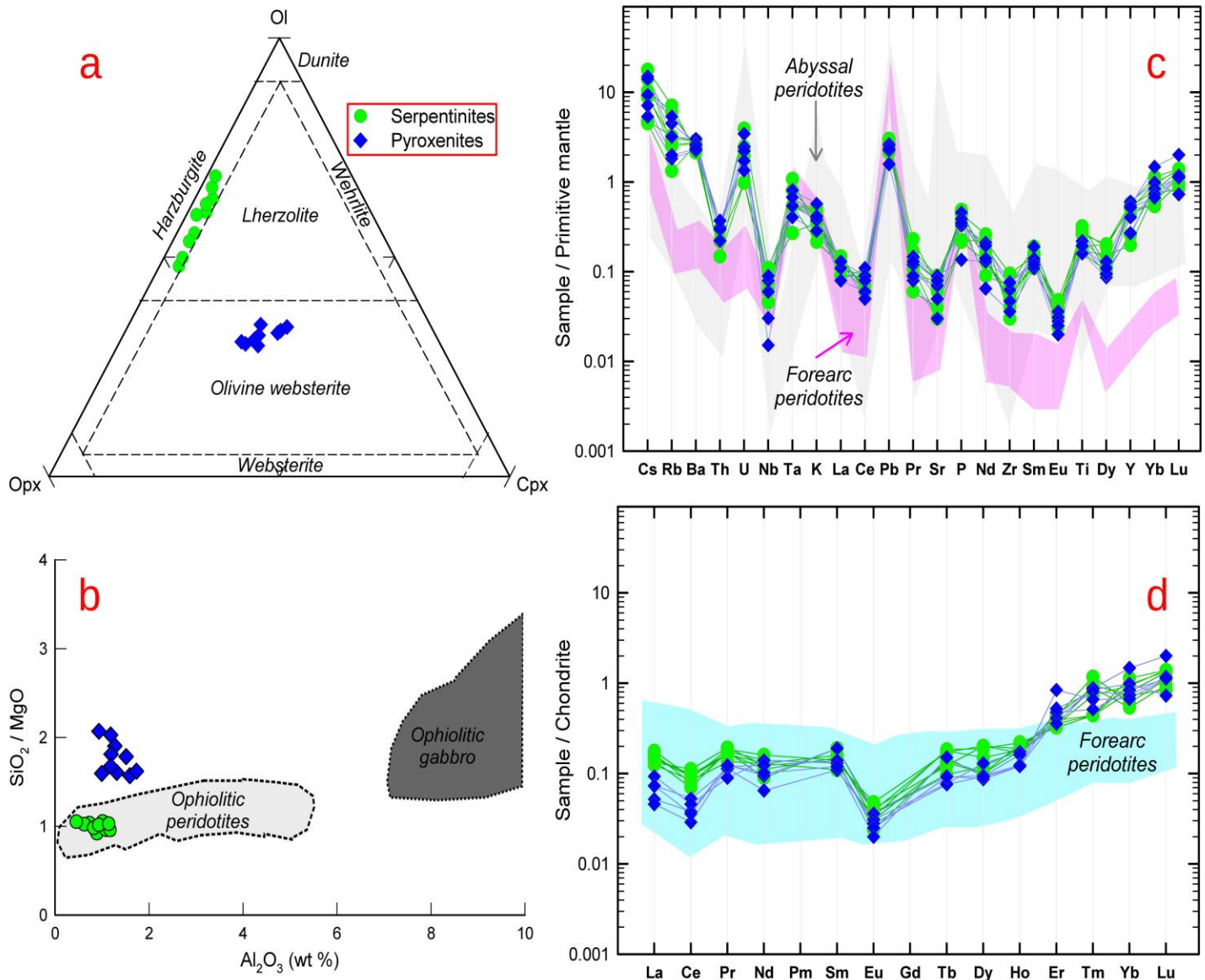


Fig. 3. (a) OI–Cpx–Opx classification diagram (Streckeisen, 1976), (b) relationship between Al_2O_3 wt.% and SiO_2 / MgO of the studied rocks (MORB, ophiolitic gabbros and ophiolitic peridotites fields after Bodinier and Godard, 2003), (c) primitive mantle-normalized trace element patterns and (d) Chondrite-normalized REE patterns for the investigated rocks (Normalizing values after McDonough and Sun 1995; Compositional ranges for ancient and modern forearc peridotites after Pearce et al., 2000 and Song et al. 2009).

The non-polarized μ -Raman spectra were recorded in the spectral range from 10 to 1200 cm^{-1} for serpentine and spinel minerals and from 3000 to 4000 cm^{-1} for serpentine minerals by using a Horiba JobinYvon RPA-HE 532 LabRAM-HR. The 632.81 nm H-Ne laser (the laser power was attenuated to 10%) with $> 500 : 1$ polarization extinction was focused with a $100\times/0.80$ objective on the sample surface. To enhance the OH stretching signal of the H_2O molecules in the high wavenumber region (3000 to 4000 cm^{-1}), the 473.10 nm doubled Nd:YAG diode laser was used. To avoid heating effects, the laser was additionally slightly defocused. The 180° backscattering geometry was analyzed with a 1200 lines/mm grating monochromator data collection mode.

The minimum system resolution and the wavenumber accuracy were about 3 cm^{-1} and $\pm 1 \text{ cm}^{-1}$, respectively (both calibrated with the Rayleigh line and the 520.6 cm^{-1} Raman peak of a silica standard). Data acquisition, instrument control, baseline correction and background subtraction were performed with LabSpec 5 software (Horiba Jobin-Yvon). Based on the signal intensity, five acquisitions with 20–30 s per 'spectral window' were measured. The single bands peak centers were determined using the combined Gaussian/Lorentzian functions by PeakFit 4.12 software (Jandel Scientific Chicago, IL, USA).

4. Results

4.1. Geochemistry

The MgO contents and LOI are much higher in serpentinites compared with those in pyroxenites; whereas the higher values of CaO content occur in pyroxenites (Table 1 online). The serpentinites plot in within the harzburgite field (Fig. 3a) comparable to those of the CED and the ANS ophiolites (Azer and Stern, 2007; Stern et al., 2004; Zimmer et al., 1995), whereas the pyroxenites lie within the olivine websterite field (Fig. 3a). Similar to other CED serpentinites (Azer and Stern, 2007; Zimmer et al., 1995), KAD serpentinites and pyroxenites are closely associated or connected with the ophiolitic peridotite (Fig. 3b). Furthermore, the low and restricted range of the serpentinites CaO contents (0.59 - 0.82 wt%, Table 1 online) suggest that Ca metasomatism, which is a common feature in the Egyptian serpentinites (Stern and Gwinn, 1990), was limited.

Both serpentinites and pyroxenites show depleted to highly depleted trace elements patterns relative to the primitive mantle (Fig. 3c) and LREE-enriched patterns (Fig. 3d). The great likeness among the trace element and REE patterns of the examined rocks indicate the genetic connection of serpentinites and pyroxenites.

4.2. Mineral chemistry

4.2.1. Spinel group minerals

In agreement with optical observations (Fig. 2b, c), the investigated spinels in serpentinites are characterized by possessing three distinct mineral-chemical zones (i.e. chromian spinels, ferrian chromite and Cr-magnetite; Fig. 4a) that mark the sporadic modification from magmatic chromian spinels to altered metamorphic rims.

Magmatic chromian spinel in serpentinites is chemically characterized by Fe^{2+} -rich chromian spinel where $\text{Cr}/\text{Fe}^{2+} > 1$; $\text{Fe}^{2+\#} [= \text{Fe}^{2+}/(\text{Fe}^{2+} + \text{Mg})]$ 0.40 - 0.57, $\text{Cr}\# [= \text{Cr}/(\text{Cr} + \text{Al})]$ 0.66 to 0.97 (Table 2 online). The Cr_2O_3 (48.88 - 57.58 wt%) is negatively correlated with Al_2O_3 (9.84 to 17.02 wt%). $\text{Mg}\# [= \text{Mg}/(\text{Mg} + \text{Fe}^{2+})]$ ranges from 0.44 to 0.60 and $\text{Fe}^{3+\#} [= \text{Fe}^{3+}/(\text{Fe}^{3+} + \text{Cr} + \text{Al})]$ is < 0.10 (Table 2 online). This composition is interpreted to be characteristic for primary mantle chromian spinels (Arai et al. 2006) with no or very little post-compositional change.

It is widely accepted that primary magmatic chromian spinel alters to ferrian chromite (formerly called ferritchromite) during serpentinization, greenschist to mid-amphibolite facies metamorphism and/or hydrothermal events (e.g., Frost 1991; Mukherjee et al. 2010; Kharbush 2013). The altered spinel rims of metamorphic origin, including ferrian chromite and Cr-magnetite plot along the join of the metamorphic magnetite in the Cr-Al- Fe^{3+} triangular diagram (i.e. Cr- Fe^{3+} join according to Barnes and Roeder, 2001; Fig. 4a).

The composition of the ferrian chromite alteration product $[(\text{Fe}^{2+}, \text{Fe}^{3+}, \text{Mg}) (\text{Cr}, \text{Fe}^{3+}, \text{Fe}^{2+}, \text{Al})_2\text{O}_4]$ is characterized by high Fe^{3+} contents (0.91 – 1.36 apfu), high Cr# (0.94-0.99; due to the loss of Al_2O_3) and low Mg/Fe^{2+} (Table 3 online).

The Cr-magnetites ($\text{Cr}/\text{Fe}^{2+} < 1$; Table 4 online) display a chemical composition, similar to that described in the ferrian chromite in terms of Fe_2O_3 , Cr_2O_3 and Al_2O_3 , however, they show an enrichment in Fe_2O_3 contents (57.21 – 67.46 wt%) and low in MgO contents, due to the extensive Mg- Fe^{2+} exchange (Table 4 online). This composition is identified as a Cr-magnetite (lie along the metamorphic magnetite Cr- Fe^{3+} join, Fig. 4a) rather than primary magnetite or chromian spinel (plots along the Al- Fe^{3+} join, Fig. 4a).

4.2.2. Clinopyroxene and serpentines

Clinopyroxenes in KAD pyroxenites (Fig. 4b, Table 5 online) are mainly diopsitic and rarely augitic in composition ($\approx \text{En}_{47-50}, \text{Wo}_{44-48}, \text{Fs}_{3-7}$; Morimoto, 1988) with high Al_2O_3 (0.63– 2.55 wt.%) and Cr_2O_3 (0.16 - 0.70 wt.%) contents, confirming their primary origin (according to Nozaka, 2010).

Serpentines are highly magnesian, with Mg# ranging from 0.86 to 0.93 (Table 6 online). The analyzed serpentine contains a restricted compositional variation in SiO_2 (43.32 to 45.46 wt.%) and low Al_2O_3 (0.21–0.82 wt%), and Cr_2O_3 (0.02–0.75 wt% presumably introduced from Cr-spinel during serpentinization).

4.2.3. Chlorite

Based on the classification of Wiewióra (1990) for chlorites, all the investigated chlorites belong to the trioctahedral group (Σ octahedral cations ≈ 12 apfu, Table 7 online). Chlorite chemistry contains low Si contents (Table 7 online) and $\text{Fe}/(\text{Fe} + \text{Mg})$ ratios and reflecting a homogeneous clinocllore composition (Fig. 4c) (Hey, 1954; Zang and Fyfe, 1995). The $[\text{Al}/(\text{Al} + \text{Fe} + \text{Mg})]$ - $[\text{Mg}/(\text{Mg} + \text{Fe})]$ diagram of Laird (1988) indicate that the investigated chlorites are formed under similar

conditions or under the same specific environmental conditions (Fig. 4d). Thus, the investigated chlorites are suitable for metamorphic conditions identification during late stages of the metamorphic evolution. The chlorite formation temperature thermometers based on the temperature dependent variation of Al^{IV} site occupancy of Cathelineau and

Nieva (1985); Xie et al., (1997) and Bourdelle and Cathelineau (2015, Fig. 4e) are, therefore applied. The results reflect that chloritization occurred in all samples around 150–350 °C based on the Al^{IV} temperatures and at an average (275 ± 10°C) (Fig. 4e, Table 7 online).

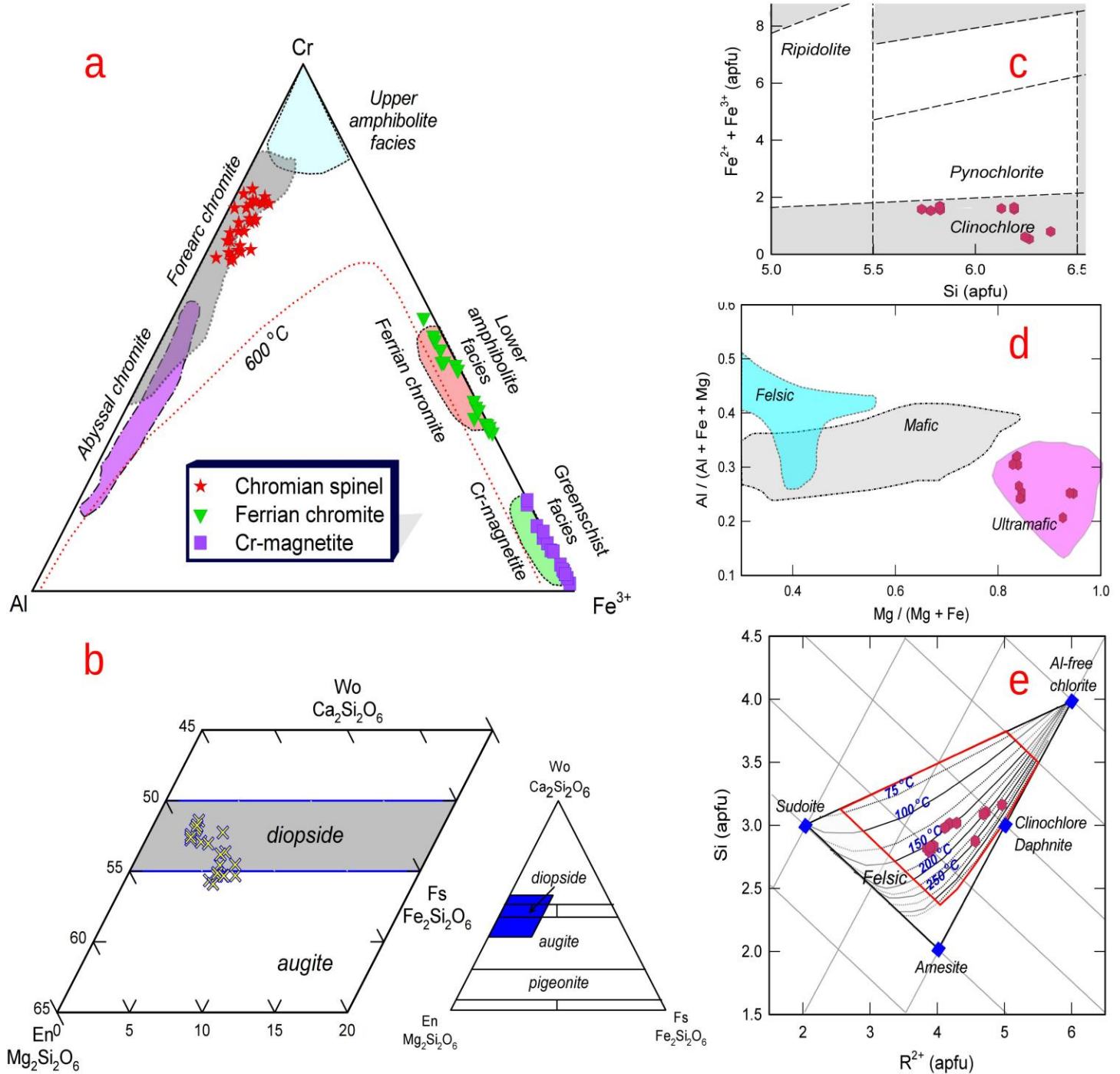


Fig. 4. (a) Composition of investigated spinel cores and rims (stability limits after Sack and Ghiorso, 1991), (b) Plot of the analyzed pyroxenes on En–Wo–Fs diagram (Morimoto, 1988), (c) chlorite classification diagram according to Hey (1954) and Zang and Fyfe (1995), (d) chlorite diagram of Laird (1988) showing the chemical composition of chlorites in various geological environments and (e) plot of chlorites on R²⁺–Si diagram of Bourdelle and Cathelineau (2015).

5. Discussion

5.1. Raman spectroscopy.

5.1.1. Serpentine group minerals

The principal minerals of the serpentine group, chrysotile, antigorite and lizardite, have a very similar chemical composition, but significantly different crystal structures. Therefore, the Raman spectroscopic technique was used to differentiate among serpentine phases. Antigorite crystallizes in the monoclinic space group C2/m (C_{2h}) with two formula units in its unit cell (Z = 2). According to Loh (1973), the spectra of serpentine minerals arose from the molecular vibrations of the distorted MgO₆ octahedra (S₆ symmetry), the distorted SiO₄ tetrahedra (C_{3v} symmetry) and the stretching and bending modes of hydroxyl group. An isolated ideal T_d symmetry tetrahedral SiO₄ group is expected to show only four Raman-active normal modes of vibration [i.e. v₁(A₁) + v₂(E) + v₃(F₂) + v₄(F₂), Nakamoto, 1997]. However, due to of intermolecular interactions, the symmetry of the SiO₄ molecule is generally lower in the crystal and thence, the SiO₄ vibrations in the crystal are controlled by a new selection rule (e.g. Kharbish 2012).

The symmetry of the SiO₄ tetrahedron in antigorite is lowered from T_d to C_{3v} site symmetry and, as a result, the

four A₁ + E + 2F₂ species will be translated into v₁(A₁) + v₂(A₁) + v₃(A₁) + v₄(E) + v₅(E) + v₆(E) modes.

Comparing the band positions and numbers of the investigated samples with those in the antigorite given by Rinaudo et al. (2003), Groppo et al. (2006) and Petriglieri et al. (2015), show a great similarity in both position and number (Table 1). Therefore the band assignments are based on the observations of the former authors (Fig. 5, Table 1). The bands occurring at 1046 and 685 cm⁻¹ were assigned to Si-O_b-Si antisymmetric v₁(A₁) and symmetric v₂(A₁) stretching vibrations, respectively (Fig. 5, Table 1). The Si-O bending modes occur at 452 cm⁻¹ v₃(A₁), 375 cm⁻¹ v₅(E) and 474 cm⁻¹ v₆(E). The weak band at 642 cm⁻¹ is assigned to the antisymmetric OH-Mg-OH translation modes (Fig. 5, Table 1). The 201 cm⁻¹ band was ascribed to Mg(O,OH)₆ group vibrations and the shoulder and band at 699 and 720 cm⁻¹, respectively were assigned to an outer Mg-OH symmetric translation mode (Fig. 5, Table 1). The libration modes of inner Mg-OH occur at 609 and 662 cm⁻¹ (Fig. 5, Table 1). The bands at 295 and 236 cm⁻¹ are assigned to v₁ (A₁) and v₂ (B₂) vibrations of the O-H-O groups (Fig. 5, Table 1).

Table 2 Raman band positions (cm⁻¹) and assignment for the spectra of proustite, smithite, trechmannite and xanthoconite in comparison with tennantite and lorandite [5], ellisite [10] and seligmannite, gratonite, sartorite, dufrénoysite and baumhauerite [2]. The minerals are sorted from left to right by increasing v₁ wavenumbers.

Attribution	Antigorite			
	This work	Groppo et al. (2006)	Petriglieri et al., (2015)	Rinaudo et al. (2003)
Hydroxyl group vibration	3693		3693	
Hydroxyl group vibration	3666		3665	
Hydroxyl group vibration	3622			
v ₁ (A ₁) Si-O _b -Si antisymmetric stretching vibrations	1046	1044	1045	1044
Outer Mg-OH symmetric translation vibration	720			
Outer Mg-OH symmetric translation vibration	699			
v ₂ (A ₁) Si-O _b -Si symmetric stretching vibration	685	683	687	683
Inner Mg-OH libration vibration	662			
Antisymmetric OH-Mg-OH translation vibration	642	635 - 640		635
Inner Mg-OH libration vibration	609			
v ₆ (E) Si-O bending vibration	474	463		
v ₃ (A ₁) Si-O bending vibration	452			
v ₅ (E) Si-O bending vibration	375	375 - 379	377	375
v ₁ (A ₁) O-H-O group vibration	295			
v ₂ (B ₂) O-H-O group vibration	236	230	229	
Mg(O,OH) ₆ group vibration	201	197 - 202		

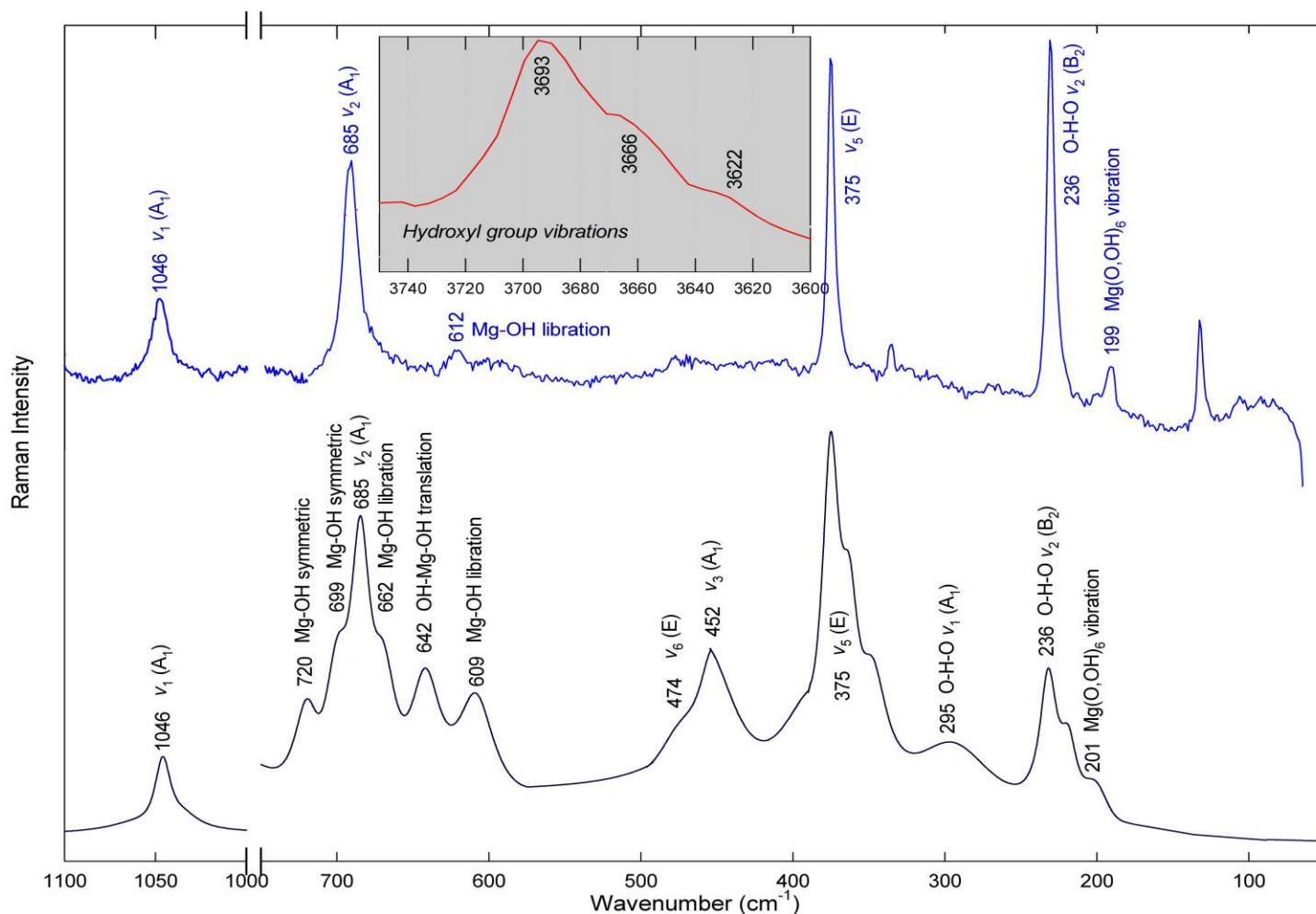


Fig. 5. Raman spectra and vibration mode positions (cm^{-1}) of the antigorite obtained by using the PeakFit program (goodness of fit $r^2 > 0.997$).

The hydroxyl group vibrations of the H_2O molecules play a definite role in the identification of the serpentine phases. The investigated antigorite shows a band triplet at 3665, 3695 and 3619 cm^{-1} , which are in good agreement with the hydroxyl group modes for the antigorite given by Petriglieri et al. (2015).

The occurrence of the Si-O_b-Si antisymmetric $\nu_1(\text{A}_1)$ band at 1046 cm^{-1} and symmetric $\nu_2(\text{A}_1)$ mode at 685 cm^{-1} have confirmed to be conclusive for the discrimination of antigorite from the other polymorphs (Rinaudo et al. 2003, Petriglieri et al. 2015). On the other hand, no characteristic modes for chrysotile (occur at 390 cm^{-1}) and lizardite (between 380 and 388 cm^{-1} , Groppo et al., 2006) were recorded. Furthermore, the speculation of serpentines as antigorite can also be indicated from the hydroxyl group modes.

5.1.2. Spinel group minerals

Spinel minerals (space group Fd-3m , O_h , $Z = 2$) have the general chemical formula AB_2O_4 , where A (e.g. Fe^{2+} , Mg^{2+}) and B (e.g. Cr^{3+} , Fe^{3+} , Al^{3+}). Spinel-type structure is based on an approximately cubic close packing of a very

compact oxygen array (anions), with cations hosted within tetrahedrally (T) and octahedrally coordinated (M) sites (D'Ippolito et al., 2015). In general, A and B cations can reside on both T and M sites, thus giving rise to a variable disorder degree, which can be described using the inversion parameter i , defined as the fraction of the B cations at the T sites. At low temperature, there are two ordered configurations, the normal spinel structure $^{\text{T}}\text{A}^{\text{M}}\text{B}_2\text{X}_4$ with $i = 0$ (e.g. chromian spinel) meaning that divalent cations enter the T site and trivalent cations the M one, and the completely inverse spinel structure $^{\text{T}}\text{B}^{\text{M}}(\text{AB})\text{X}_4$ with $i = 1$ (e.g. magnetite) (D'Ippolito et al., 2015).

The spinel primitive unit cell includes 14 atoms, therefore the number of allowable modes of spinel predicted from factor group analysis (FGA) is 42 (3 acoustic modes + 39 optical modes). In terms of irreducible representations, these modes can be decomposed as $\Gamma = \text{A}_{1g}(\text{R}) + 2\text{A}_{2u} + \text{E}_g(\text{R}) + 2\text{E}_u + \text{F}_{1g} + 5\text{F}_{1u}(\text{IR}) + 3\text{F}_{2g}(\text{R}) + 2\text{F}_{2u}$, leading to 5 active optical modes in Raman spectroscopy (i.e. $\text{A}_{1g} + \text{E}_g + 3\text{F}_{2g}$). The (R) and (IR) identify Raman-active and infrared-active vibrational modes, respectively, and the rest of the species are silent modes. The E and F modes are doubly and triply degenerate, respectively and the three acoustic

modes belong to the F_{1u} species. FGA of the examined spinel was performed on the Bilbao Crystallographic Server (<http://www.cryst.ehu.es/>).

The investigated spinels exhibit Raman vibrational modes in the spectral region $800-100\text{ cm}^{-1}$, with no additional bands occur in higher energy regions (Fig. 6, Table 2). The low wavenumber limit of the considered spinels spectra was chosen only by the cut-off value of the used Raman edge and notch filters. In the spectrum of the studied magmatic chromian spinel cores (Fig. 6, Table 2), the strongest band at 691 cm^{-1} corresponds to A_{1g} mode (Wang et al., 2004). The medium to weak intensity bands at 601 , 555 and 197 cm^{-1} correspond to modes F_{2g} (3), F_{2g} (2)

and F_{2g} (1), respectively (Reddy and Frost, 2005). The weak mode at 475 cm^{-1} was assigned to the E_g species (D'Ippolito et al., 2015).

The Raman spectra of the ferrian chromite are also similar and correspond to the spectra of magmatic chromian spinel cores (Fig. 6, Table 2). However, the bands display blue shift (i.e. increase in wavenumber or in energy) and changes in peak intensity and shape. Furthermore, additional weak bands and shoulders occur around their major Raman peaks at 646 and 570 cm^{-1} , beside the five predicted Raman active modes for the spinel structure (Fig. 6, Table 2).

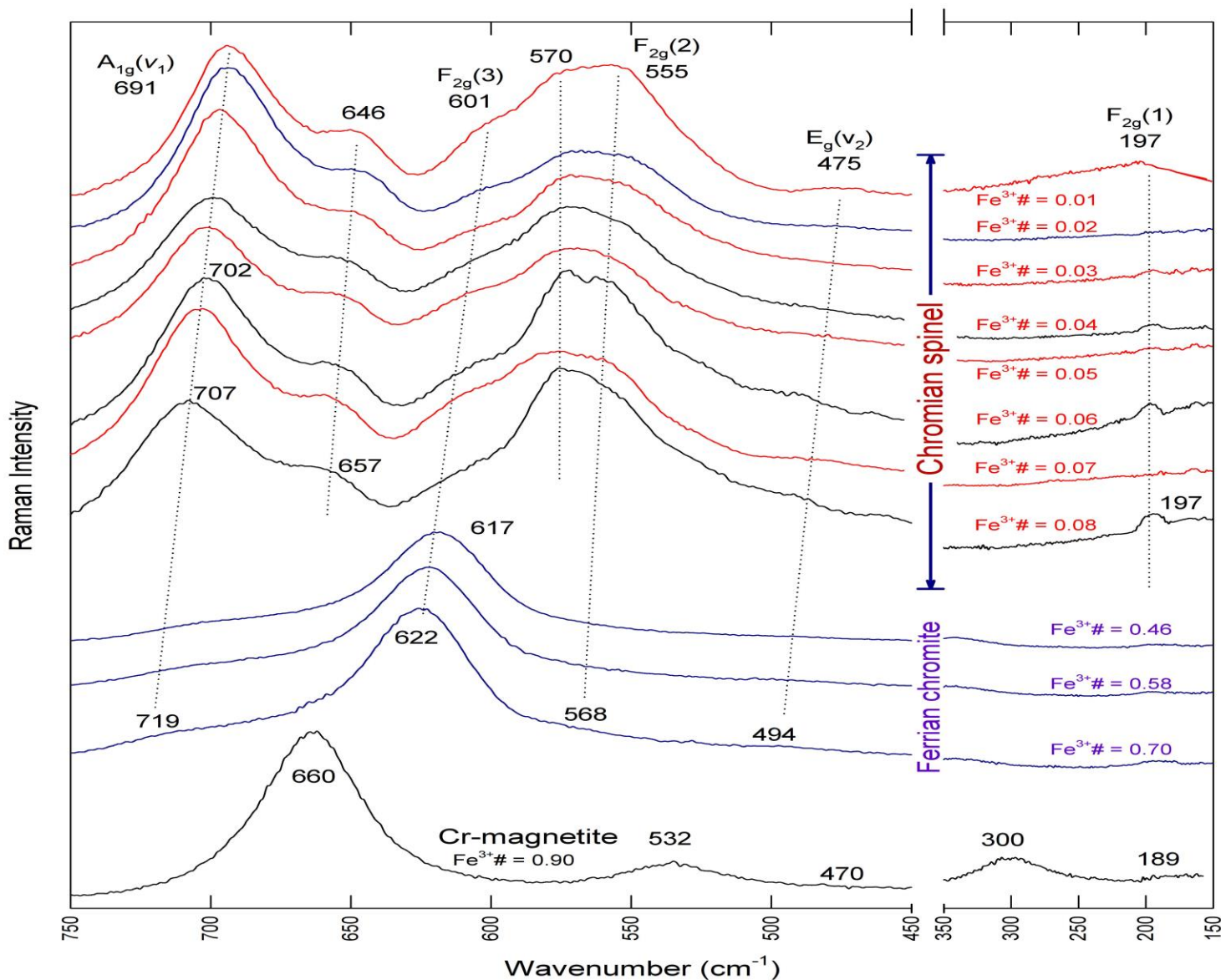


Fig. 6. Raman spectra and vibration mode positions (cm^{-1}) of the chromian spinel, ferrian chromite and Cr-magnetite obtained by using the PeakFit program ($r^2 > 0.998$).

Table 2 Raman band positions (cm^{-1}) and assignment for the spectra of proustite, smithite, trechmannite and xanthoconite in comparison with tennantite and lorandite [5], ellisite [10] and seligmannite, gratonite, sartorite, dufrénoysite and baumhauerite [2]. The minerals are sorted from left to right by increasing ν_1 wavenumbers.

	Antigorite		SMITHITE				
	A_{1g}	F_{2g} (3)	cm^{-1}				
			F_{2g} (2)	E_g	F_{2g} (1)		
	691	646	601	570	555	475	197
	692	647	603	570	556	476	198
	695	650	605	571	557	478	197
	699	651	607	572	560	480	199
	700	653	610	573	563	480	200
	702	654	613	575	563	483	95
	704	655	615		564	485	199
	707	657	618		565	486	197
	715		620		567	492	197
	717		622		568	494	197
	719		625		570	495	198
Wang et al., (2004)	690		650		600	445	-
Reddy and Frost (2005)	730		-		560	445	
D'Ippolito et al., (2015)	684		612		542	446	
	660		532		470	300	189
Shebanova and Lazor (2003) and references therein	668		538		-	306	193
	669		540		410	300	-
	666		541		-	311	-

The Raman spectra of Cr-magnetite display also five weak to strong bands: 660 (A_{1g}), 532 [F_{2g} (3)], 470 [F_{2g} (2)], 300 (E_g), and 189 [F_{2g} (1)] cm^{-1} , which correspond to the theoretical active modes of magnetite reported in different studies (Table 2), but are shifted to lower frequencies. The shift in peak position in Cr-magnetite to lower frequencies relative to the reported studies is probably caused by the incorporation of Cr admixture into the crystal structure (Cr_2O_3 , 0.94-10.78 wt% Table 4 online).

The band at 555 cm^{-1} (F_{2g}) in chromian spinel is shifted to 570 cm^{-1} (viz. higher frequencies) ferrian chromite and is much weaker than the corresponding band in the spectrum of the chromian chromite (Figs. 6, 7). According to Reddy and Frost (2005) this band characterizes the vibrations of trivalent cations including those of the Cr^{3+} ions at M sites. This observation reflects directly the higher Cr content (> 48 wt %) in chromian spinel relative to that from that from the ferrian chromite (< 35 wt %). Moreover, the E_g peak position (475 cm^{-1} in chromian spinel, shifted to 495 cm^{-1} in ferrian chromite Figs, 6, 7) is a distinctive of chromian spinel changed to ferrian type (according to D'Ippolito et al. 2015).

Moreover, according to the Hooke's law and the classical harmonic oscillator model (i.e. stronger bonds and lighter atoms result in higher stretching frequencies), the peak shifts is also attributed to the probable differences in the band positions that arise from variations in spinel chemistry (i.e. substitution in T and M sites) and also to the difference in atomic mass of Cr, Al and Fe.

Figure 7 reflects, in addition to the above observations, that (1) the vibrational mode positions depend on increasing the proportion of Fe^{3+} and (2) the modes at 646 and 570 cm^{-1} are restricted to chromian spinel (cores). In addition, the cation substitution in T and M sites causes local distortions in the crystal structure and hence, a symmetry lowering from D_{3d} to C_{3v} and a crystal structure change from O_h to T_d . The lowering in the symmetry increases the total number of Raman active (and / or IR) modes in the spinel spectra (Grimes and Collett 1971).

From the above discussion, it can be speculated that the change in the chemistry for the spinel core and rim samples obtained from interpretation of the Raman spectra agree with the EMP analysis and SEM results and indicate the systematic change in the spinel chemistry from core to rim.

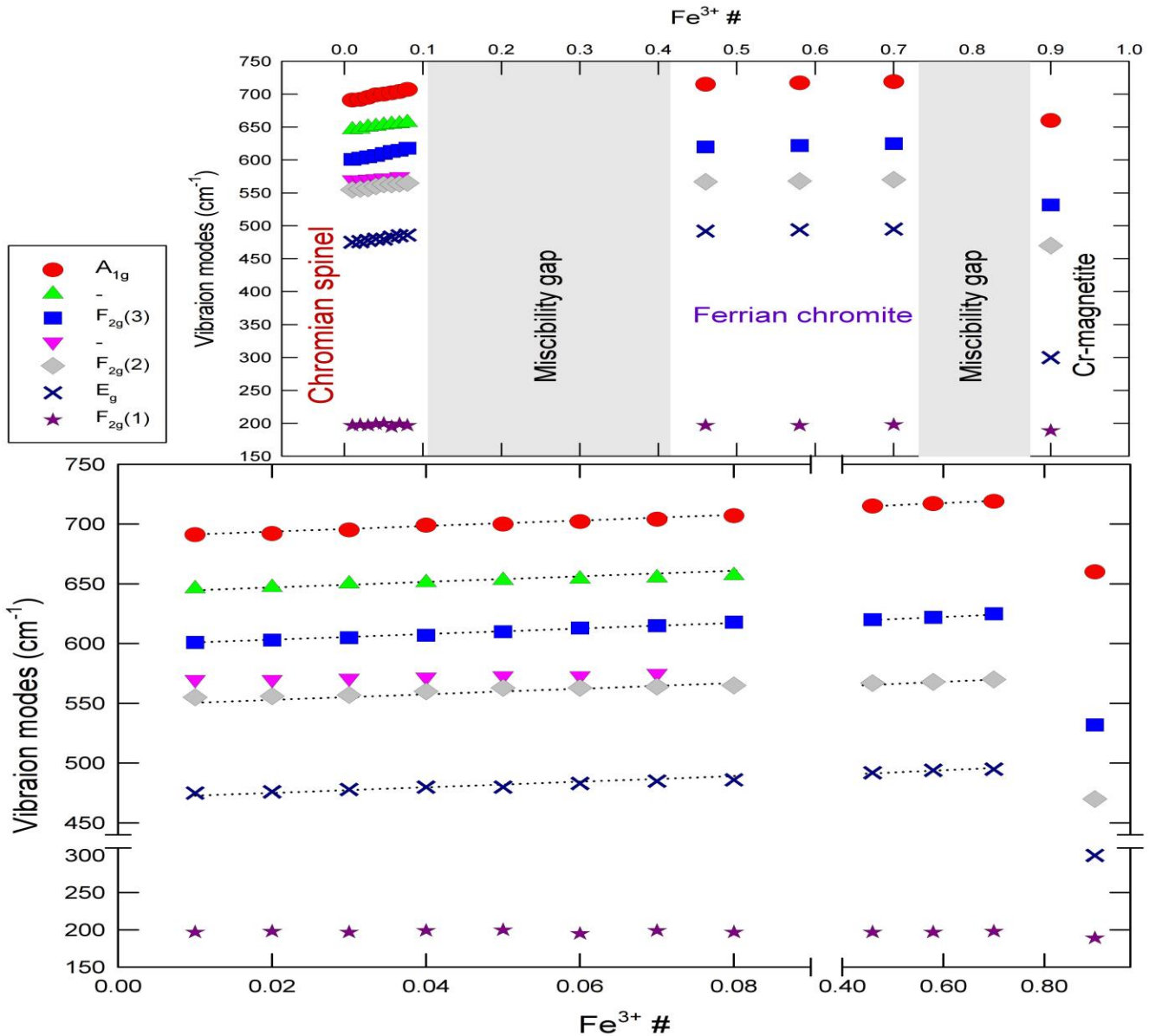


Fig. 7. Correlation between the Raman mode positions of the chromian spinel, ferrian chromite and Cr-magnetite and Fe³⁺#.

5.2. Magma type and tectonic setting

The low Al₂O₃ and CaO contents (Fig 8a) of studied serpentinites together with the low Ti and high Cr# (Fig. 8b, c) and Mg# (Fig. 8d) in the chromian spinel cores confirm their boninitic affinity and their similarity to the ophiolitic forearc peridotites worldwide and in ANS (Azer and Stern, 2007; Khalil and Azer, 2007; Stern et al., 2004). Furthermore, the chemistry of clinopyroxenes in pyroxenites reflect their strong affinity toward the intra-oceanic forearc boninites (Figs. 9a, b).

The Al₂O₃ contents and the FeO/MgO ratio of the parental melt and the empirical degree of partial melting (F) of the investigated chromian spinels in serpentinites were computed using the equations of Maurel and Maurel (1982) and Hellebrand et al., (2001), respectively.

The obtained values (Table 2 online) of the parental melt Al₂O₃ (10.31 – 12.89 wt%), FeO/MgO (0.95 – 1.84) and F (19 - 22) are consistent with the composition of primary boninites [Al₂O₃ = 10.60–14.40 wt%, FeO/MgO = 0.70 – 1.40, (Wilson, 1989)] and the peridotites recovered from forearcs (F = 20-25; Zanetti et al., 2006).

Furthermore, the depletion in Nb contents (Fig. 3c) are similar to those in the forearc peridotites (Niu, 2004; Song et al., 2009). The REE patterns of KAD show great similarity with those of modern forearc peridotites especially from the South Sandwich (Pearce et al., 2000) (Fig. 3d).

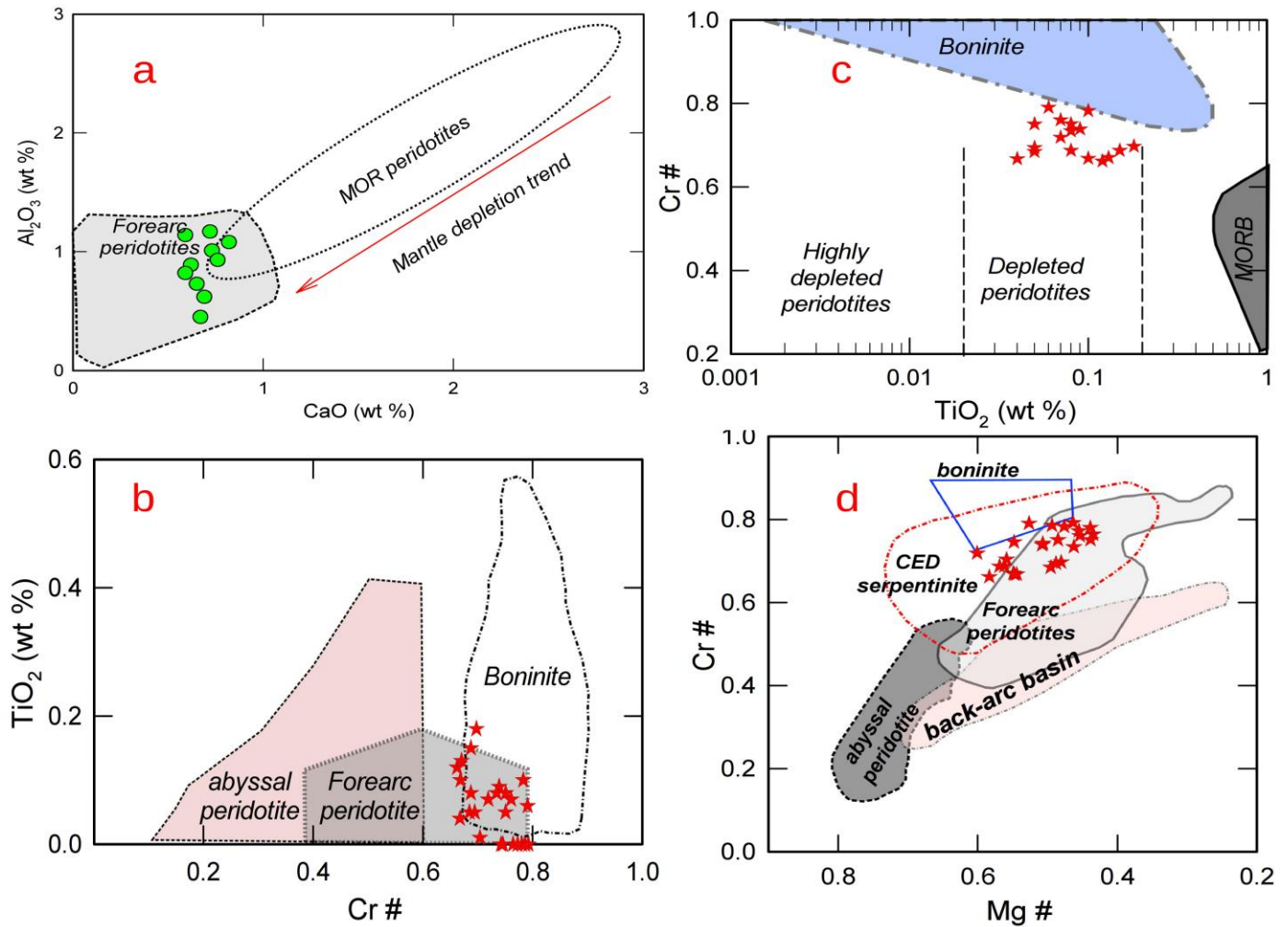


Fig. 8. (a) CaO vs. Al_2O_3 diagram showing the studied serpentinites compared with MOR and forearc peridotites (after Ishii et al., 1992), symbols as in Fig. 3a, chromian spinel composition plotted on (b) Cr# vs. TiO_2 (Fields after Dick and Bullen, 1984), (c) Cr# vs. TiO_2 diagram (fields after Dick and Bullen, 1984; Jan and Windley, 1990) and (d) Mg# vs. Cr# (after Stern et al., 2004) showing various tectonic regime fields (after Bloomer et al., 1995; Dick and Bullen, 1984). CED field for chromites in the Central Eastern Desert serpentinites is from Farahat et al. (2011), symbols as in Fig. 4a

5.3. Alteration and thermal history

One of the fundamental problems related to the study of serpentinites is the determination of their metamorphic grade.

The presence of antigorite as the only serpentine mineral (see Raman spectroscopy part) in serpentinites and the absence of newly formed olivine indicates that they were formed in the stability field of antigorite (250–600 °C; Evans 2004) or that the temperature did not exceed the lower amphibolite facies metamorphism range (i.e. below 500°C). Serpentinites have been most likely formed directly from mantle-wedge olivine above the slab in which the fluids driven for the slab cause strong hydration and cooling of peridotites during an early stage of serpentinization (400–600 °C; Khedr and Arai 2010). Thus the antigorite formation usually occur at ~ 500°C (Moody, 1976), while the olivine after antigorite is commonly

composed by dehydration at > 500°C; (Caruso and Chernosky, 1979), which is the minimum temperature for the ferrian chromite, antigorite and chlorite formation (Jan and Windley, 1990).

Figure 9c shows that the chromian spinel core compositions are in equilibrium with Fo_{88} and Fo_{94} olivines (the typical range of komatiitic olivines) at temperatures around 1100°C and 750°C, respectively. These high equilibrium temperatures indicate that the chromian spinel cores are relics of the original igneous cooling stage, and have not been changed during subsequent metamorphism or alteration. Many researchers have proposed that chromian spinel breakdown during metamorphism to form chlorite (Shen et al., 1988) at relatively high temperatures (> 400°C; Kimball 1990) and in the presence of aqueous fluids (Merlini et al., 2009); implies outward Al and Mg diffusion from chromian spinel, leaving a residual Fe^{3+} -

enriched and Al-, Mg-depleted Cr-spinel (ferrian chromite) (Kimball, 1990; Merlini et al., 2009). The serpentinization of both pyroxene and olivine at temperatures between 200 and 300° C (Bach et al., 2006) could favor the creation of an aqueous fluid rich environment necessary for the chlorite and ferrian chromite formations.

The progressive increase in Fe³⁺ and depleted in Mg in the investigated chromian spinel from core to rim (Tables 2, 3 online, see also Raman spectroscopy part) suggests a change in the alteration conditions to more oxidative states with increasing metamorphism (Anzil et al., 2012). At high oxidative conditions [i.e. increase in f(O₂)], the reaction of chromian spinel with serpentine favor to produce chlorite and Cr-magnetite (Mellini et al., 2005). This increase in the oxidative conditions (necessary for Cr-magnetite formation) may be took place after the late stages of serpentinization

or during lower temperature amphibolite facies metamorphism (Bach et al., 2006). The Irvine's spinel prism (Irvine, 1965) indicates that the f(O₂) for the chromian spinel is relatively low, whereas the ferrian chromite was formed under relatively high f(O₂), which increases upward to produce Cr-magnetite (Fig. 9d).

Furthermore, there is a miscibility gap between chromian spinel and ferrian chromite / Cr-magnetite (rims) corresponding to metamorphism around ~500- 600° C (Fig. 4a) and there is no complete solid solution between ferrian chromite and Cr-magnetite (Fig 4a), which reflects the incomplete re-equilibration between chromian spinel and its alteration products in lowest amphibolite facies (i.e. around 500- 600°C).

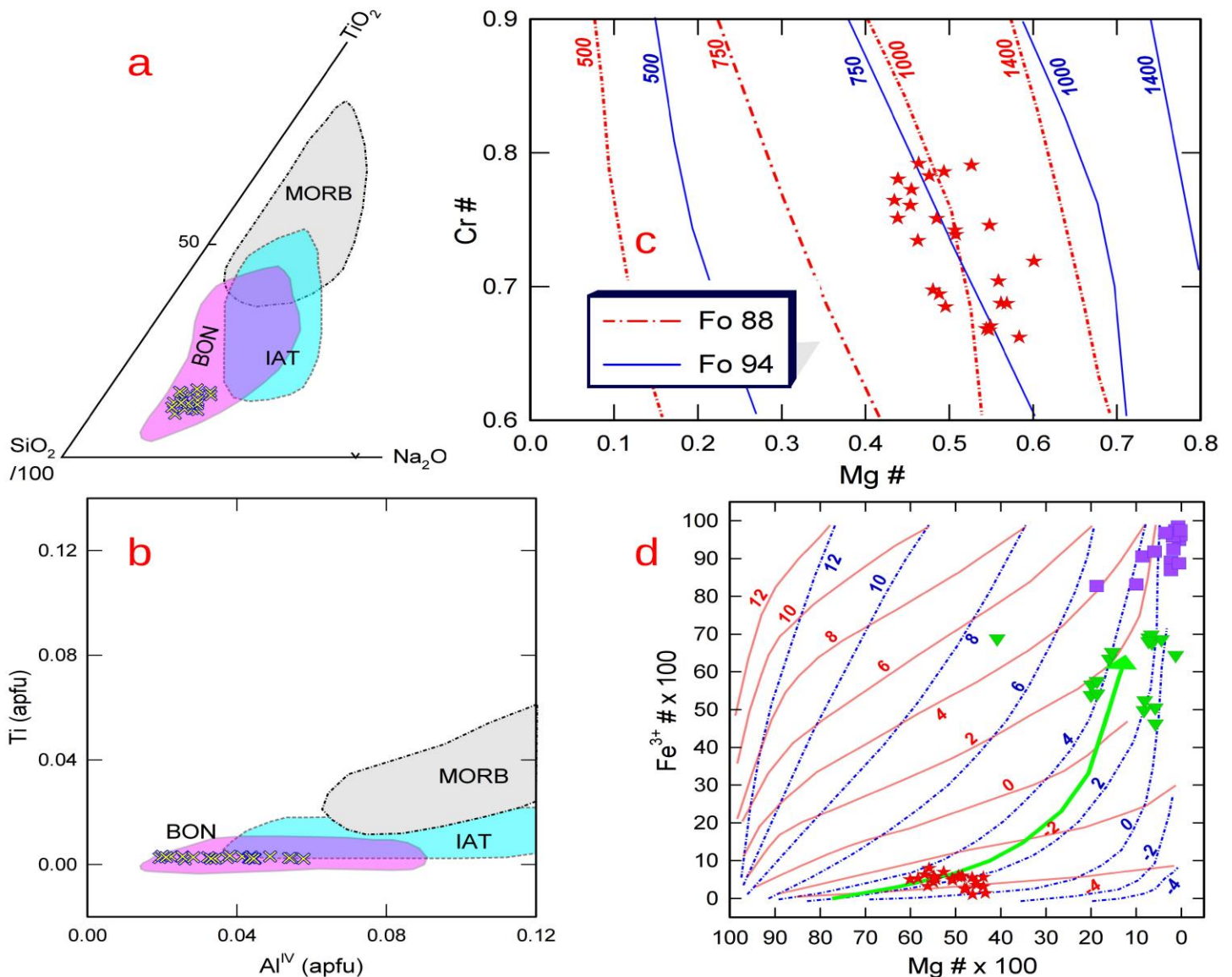


Fig. 9. Plot of the analyzed pyroxenes on (a) SiO₂ –TiO₂ –Na₂O diagram (Beccaluva et al., 1989), (b) Ti vs. Al^{IV} diagram (Beccaluva et al., 1989), (c) chromian spinel compositions in equilibrium with Fo₉₄ and Fo₈₈ olivine at different temperatures (Barnes, 2000; Sack and Ghiorso, 1991), (d) plot of Fe³⁺# vs. Mg# in spinel phases (oxygen fugacity isobars after Irvine, 1965); light green arrow represents the compositional trend of some Egyptian chromites.

In addition, the presence of a compositional gap between ferrian chromite and Cr-magnetite, which widens rapidly below 550°C (Barnes, 2000) and disappears above 600°C (Sack and Ghiorso, 1991), reflects their formation during the lower amphibolite facies. A further evidence can be elicited from the Mg and Fe²⁺ of ferrian chromite and Cr-magnetite (Tables 3, 4 online), which is matched with those of the lower amphibolite facies metamorphism given by Barnes (2000). The chlorite geothermometry add another clue, in which proposes temperatures between 150° and 350°C for the serpentinization-chloritization processes.

5.4. Genesis of pyroxenites

The investigated pyroxenites display a very close relation to the serpentinites in term of mineral chemistry, trace elements (Fig 3c) and REE (Fig. 3d) geochemistry, which reflect that both are co-genetic with the rest of the mantle suite. Therefore, the KAD pyroxenites genesis could be related to the contamination of their mantle source by crustal material and/or subduction-related slab fluids during mantle evolution in supra subduction zone (SSZ) setting. Thus the low TiO₂ contents (0.07 -0.12 wt%, Table 1 online), the enrichment in LILE (Fig 3c) and LREE (Fig. 3d) and the Nb depletion (Fig. 3c) indicate the remelting of a highly depleted mantle source (Sun and Nesbitt, 1978) and suggest their formation in a SSZ environment (i.e forearc).

References

- Ali-Bik, M.W., Taman, Z., El Kalioubi, B., Abdel Wahab, W., 2012. Serpentine-hosted talc–magnesite deposits of Wadi Barramiya area, Eastern Desert, Egypt: Characteristics, petrogenesis and evolution. *Journal of African Earth Sciences* 64, 77–89.
- Andráš, P., Kharbish, S., 2014. Gold sources in ancient Egypt. In: Andráš, P., Dimer, V., Kharbish, S. (Eds), *Historic deposits and their impact on environment*. 1st Ed., Technicka univerzita v Kosiciach Slovakia, ISBN 978-80-553-1756-4, 57-75.
- Anzil, P.A., Guerreschi, A.B., Martino, R.D., 2012. Mineral chemistry and geothermometry using relict primary minerals in the La Cocha ultramafic body: a slice of the upper mantle in the Sierra Chica de Cordoba, Sierras Pampeanas, Argentina. *Journal of South American Earth Sciences* 40, 38–52.
- Arai, S., Shimizu, Y., Ismail, S.A., Ahmed, A.H., 2006. Low-T formation of high-Cr spinel with apparently primary chemical characteristics within podiform chromitite from Rayat, northeastern Iraq. *Mineralogical Magazine* 70, 499–508.
- Azer, M.K., Stern, R.J., 2007. Neoproterozoic (835–720 Ma) serpentinites in the Eastern Desert, Egypt: fragments of forearc mantle. *The Journal of Geology* 115, 457–472.
- Bach, W., Paulick, H., Garrido, C.J., Ildefonse, B., Meurer, W., Humphris, S.E., 2006. Unravelling the sequence of serpentinization reactions: petrography, mineral chemistry, and petrophysics of serpentinites from MAR 15oN (ODP Leg 209, Site 1274). *Geophysical Research Letters* 25, 1467-1470.
- Barnes, S.J., 2000. Chromite in komatiites II. Modification during green-schist to mid-amphibolite facies metamorphism. *Journal of Petrology* 41, 387–409.
- Barnes, S.J., Roeder, P.L., 2001. The range of spinel compositions in terrestrial mafic and ultramafic rocks. *Journal of Petrology* 42, 2279–2302.
- Beccaluva, L., Macciota, G., Piccardo, G.B., Zeda, O., 1989. Clinopyroxene composition of ophiolitic basalts as petrogenetic indicator. *Chemical Geology* 77, 165–182.
- Bloomer, S.H., Taylor, B., MacLeod, C.J., Stern, R.J., Fryer, P., Hawkins, J.W., Johnson, L., 1995. Early arc volcanism and ophiolite problem: a perspective from drilling in the Western Pacific. In: Taylor, B., Natland, J. (Eds.), *Active Margins and Marginal Basins of the Western Pacific*, Geophysical Monograph, 88. American Geophysical Union, Washington, DC, pp. 1–30.
- Bodinier, J.L., Godard, M., 2003. Orogenic, ophiolitic, and abyssal peridotites. In: Carlson, R.W. (Ed.), *Treatise on Geochemistry Mantle and core: Treatise on Geochemistry 2*. Elsevier Science Ltd, 103–170.
- Bourdelle, F., Cathelineau, M., 2015. Low-temperature chlorite geothermometry: a graphical representation based on a T–R²⁺–Si diagram. *European Journal of Mineralogy* 27, 617–626.
- Caruso, L.J., Chernosky, J.V. Jr., 1979. The stability of lizardite. *Canadian Mineralogist* 17, 757–770.
- Cathelineau, M., Nieva, D., 1985. A chlorite solid solution geothermometer The Los Azufres (Mexico) geothermal system. *Contributions to Mineralogy and Petrology* 91, 235-244.
- D'Ipollito, V., Andreozzi, G.B., Bersani D., Lottici, P.P., 2015. Raman fingerprint of chromate, aluminate and ferrite spinels. *Journal of Raman Spectroscopy* 46, 1255–1264.
- Dick, H.J.B., Bullen, T., 1984. Chromian spinel as a petrogenetic indicator in abyssal and alpine type peridotites and spatially associated lavas. *Contribution to Mineralogy and Petrology* 86, 5–76.
- Evans, B.W., 2004. The Serpentine Multisystem Revisited: Chrysotile Is Metastable. *International Geology Review* 46, 479–506.
- Farahat, E.S., El-Mahalawi, M.M., Hoinkes, G., 2004. Continental back-arc basin origin of some ophiolites from the Eastern Desert of Egypt. *Mineralogy and Petrology* 82, 81–104.
- Farahat, E.S., Hoinkes, G., Mogessie, A., 2011. Petrogenetic and geotectonic significance of Neoproterozoic suprasubduction mantle as revealed by the Wizer ophiolite complex, Central Eastern Desert, Egypt. *International Journal of Earth Sciences* 100, 1433
- Frost, B.R., 1991. Stability of oxide minerals in metamorphic rocks. In: Lindsley, R.H. (Ed) *Oxide minerals: petrologic and magnetic significance*. *Reviews in Mineralogy and Geochemistry* 25, 469-488.
- Gaafar, I., Aboelkhair, H., 2014. Analysis of Geological and Geophysical Datasets for Radioelement Exploration in Kab Amiri Area, Central Eastern Desert, Egypt. *The Open Geology Journal* 8, 34-53.
- Grimes, N.W., Collett, A.J., 1971. Correlation of infrared spectra with structural distortions in the spinel series Mg (Cr_xAl_{2-x})O₄. *Physica Status Solidi B: Basic Research* 43, 591–599.
- Gropo, C., Rinaudo, C., Cairo, S., Gastaldi, D., Compagnoni, R., 2006. Micro-Raman spectroscopy for a quick and reliable identification of serpentine minerals from ultramafics. *European Journal of Mineralogy* 18(3), 319 – 329.
- Hellebrand, E., Snow, J.E., Dick, H.J.B., Hofmann, A.W., 2001. Coupled major and trace elements as indicators of the extent of melting in mid-ocean-ridge peridotites. *Nature* 410, 677-681.
- Hey, M.H., 1954. A new review of the chlorites. *Mineralogical Magazine* 30, 277–292.
- Irvine, T.N., 1965. Chromian spinel as a petrogenetic indicator. part I. theory. *Canadian Journal of Earth Sciences* 2, 648-672.

- Ishii, T., Robinson, P.T., Maekawa, H., Fiske, R., 1992. Petrological studies of peridotites from diapiric serpentinite seamounts in the Izu–Ogasawara–Mariana forearc, leg 125. In: Pearce, J., Stokking, L.B., et al. (Eds.), *Proceedings of the Ocean Drilling Project, Leg 125, Scientific Results (College Station)*, pp. 445–485.
- Jan, M.Q., Windley, B.F., 1990. Chromian spinel-silicate chemistry in ultramafic rocks of the Jijal Complex, northwest Pakistan. *Journal of Petrology* 31, 67–71.
- Khalil, A.E.S., Azer, M.K., 2007. Supra-subduction affinity in the Neoproterozoic serpentinites in the Eastern Desert, Egypt: evidence from mineral composition. *Journal of African Earth Sciences* 49, 136–152.
- Kharbish, S., 2007. A Raman spectroscopic investigation of Fe-rich sphalerite: effect of Fe-substitution. *Physics and Chemistry of Minerals* 34/8, 551-558.
- Kharbish, S. 2011. Raman spectroscopic investigations of some Ti-sulfosalts minerals containing pyramidal (As,Sb)S₃ groups. *American Mineralogist* 96, 609-616.
- Kharbish, S., 2012. Raman spectra of minerals containing interconnected As(Sb)O₃ pyramids: Trippkeite and schafarzikite. *Journal of GEOsciences* 57, 51–60.
- Kharbish, S., 2013. Metamorphism and Geochemical aspects on Neoproterozoic serpentinites hosted chrome spinel from Gabal Al-Degheimi, Eastern Desert, Egypt. *Carpathian Journal of Earth and Environmental Sciences* 8/4, 125–138.
- Kharbish, S., 2016. Micro-Raman spectroscopic investigations of extremely scarce Pb-As sulfosalt minerals: baumhauerite, dufrénoyite, gratonite, sartorite and seligmannite. *Journal of Raman Spectroscopy* 47, 1360-1366.
- Kharbish, S., 2017. Spectral-structural characteristics of the extremely scarce silver arsenic sulfosalts, proustite, smithite, trechmannite and xanthoconite: μ -Raman spectroscopy evidence. *Spectrochimica Acta Part A: Molecular and Biomolecular Spectroscopy* 177, 104-110.
- Kharbish, S., Andráš, P., 2014a. Exploitation of ores, rocks and minerals in ancient Egypt. *Acta Universitatis Matthiae Belli, seria Environmentalne Manazerstov* 1, 24-33.
- Kharbish, S., Andráš, P., 2014b. Pharaonic Egypt mines and quarries. In: Andráš, P., Dimer, V., Kharbish, S. (Eds), *Historic deposits and their impact on environment*. 1st Ed., Technicka univerzita v Kosiciach Slovakia, ISBN 978-80-553-1756-4, 36 - 57.
- Kharbish, S., Andráš, P., 2014c. Investigations of the Fe sulfosalts berthierite, garavellite, arsenopyrite and gudmundite by Raman spectroscopy, *Mineralogical Magazine* 78(5), 1287–1299.
- Kharbish, S., Jeleň, S., 2016. Raman spectroscopy of the Pb-Sb sulfosalts minerals: boulangerite, jamesonite, robinsonite and zinkenite, *Vibrational Spectroscopy* 85, 157–166.
- Kharbish S., Andráš, P., Luptáková, J., Milovská, S., 2014. Raman spectra of oriented and non-oriented Cu hydroxy-phosphate minerals: Libethenite, cometite, pseudomalachite, reichenbachite and ludjibaite. *Spectrochimica Acta Part A: Molecular and Biomolecular Spectroscopy* 130, 152-163.
- Kharbish, S., Libowitzky, E., Beran, A., 2007. The effect of As-Sb substitution in the Raman spectra of tetrahedrite-tennantite and pyrargyrite-proustite solid solutions. *European Journal of Mineralogy* 19/4, 567-574.
- Kharbish, S., Libowitzky, E., Beran, A. 2009. Raman spectra of isolated and interconnected pyramidal XS₃ (X = Sb,Bi) groups in stibnite, bismuthinite, kermesite, stephanite and bournonite. *European Journal of Mineralogy* 21/2, 325-333.
- Khedr, M.Z., Arai, S., 2010. Hydrous peridotites with Ti-rich chromian spinel as a low-temperature forearc mantle facies: evidence from the Happo-O'ne metaperidotites (Japan). *Contribution to Mineralogy and Petrology* 159, 137–157.
- Kimball, K.L., 1990. Effects of hydrothermal alteration on the composition of chromian spinels. *Contributions to Mineralogy and Petrology* 105, 337-346.
- Kuebler, K.E., Wang, A., Abbott, K., Haskin, L.A., 2001. Can we detect carbonate and sulfate minerals on the surface of Mars by Raman spectroscopy? Abstract No. 1889. *Lunar and Planetary Science XXXII*, Lunar and Planetary Institute, Houston, Texas.
- Kuebler, K.E., Jolliff, B.L., Wang, A., Haskin, L.A., 2002. A Raman spectroscopic study of samples from the May 2001 FIDO test site, Abstract no. 1536. *Lunar and Planetary Science XXXIII*, Lunar and Planetary Institute, Houston, Texas.
- Laird, J., 1988. Chlorites: metamorphic petrology. In: Bailey, S.W. (Ed), *Hydrous Phyllosilicates (Exclusive of Micas)*. *Reviews in Mineralogy* 19, 405-454.
- Loh, E., 1973. Optical vibrations in sheet silicates. *Journal of Physics C: Solid State Physics* 6(6), 1091 – 1104.
- Maurel, C., Maurel, O., 1982. Étude expérimentale de la distribution de l'aluminium entre bain silicaté basique et spinelle chromifère. Implications pétrogénétiques: teneur en chrome des spineless. *Bulletin de Minéralogie* 105, 197-202.
- McDonough, W.F., Sun, S.-s., 1995. The composition of the earth. *Chemical Geology* 120, 223–253.
- Mellini, M., Rumori, C., Viti, C., 2005. Hydrothermally reset magmatic spines in retrograde serpentinites: formation of "ferritchromit" rims and chlorite aureoles. *Contributions to Mineralogy and Petrology* 149, 266-275.
- Merlini, A., Grieco, G. & Diella, V., 2009. Ferritchromite and chromian-chlorite formation in mélange-hosted Kalkan chromitite (Southern Urals, Russia). *American Mineralogist* 94, 1459–1467.
- Moghazi, A.M., 2002. Petrology and geochemistry of Pan-African granitoids, Kab Amiri area, Egypt – implications for tectonomagmatic stages in the Nubian Shield evolution. *Mineralogy and Petrology* 75, 41–67.
- Moody, J.B., 1976. Serpentinization: a review. *Lithos* 9, 125–138.
- Morimoto, N., 1988. Nomenclature of pyroxenes. *Mineralogy and Petrology* 39, 55–76.
- Mukherjee, R., Mondal, S.K., Rosing, M.T., Frei, R., 2010. Compositional variations in the Mesoarchean chromitites of the Nuggihalli schist belt, Western Dharwar Craton (India): potential parental melts and implications for tectonic setting. *Contributions to Mineralogy and Petrology* 164, 179–192.
- Nakamoto, K. (1997): *Infrared and Raman spectra of inorganic and coordination compounds*. Part A: theory and applications in inorganic chemistry. 5th ed., Wiley-Interscience, New York, 408 p.
- Niu, Y., 2004. Bulk-rock major and trace element compositions of abyssal peridotites: implications for mantle melting melt extraction and post-melting processes beneath mid-ocean ridges. *Journal of Petrology* 45 (12), 2423–2458.
- Nozaka, T., 2010. A note on compositional variation of olivine and pyroxene in thermally metamorphosed ultramafic complexes from SW Japan. *Okayama University, Earth Science Reports* 17 (1), 1–5.
- Pearce, J.A., Barker, P.F., Edwards, S.J., Parkinson, I.J., Leat, P.T., 2000. Geochemistry and tectonic significance of peridotites from the south sandwich arc-basin system, South Atlantic. *Contributions to Mineralogy and Petrology* 139, 36–53.
- Petriglieri, J.R., Salvioli-Mariani, E., Mantovani, L., Tribaudino, M., Lottici, P.P., Laporte-Magoni, C., Bersani, D., 2015. Micro-Raman

- mapping of the polymorphs of serpentine. *Journal of Raman Spectroscopy* 46, 953–958.
- Reddy, B.J., Frost, R.L., 2005. Spectroscopic characterization of chromite from the Moa-Baracoa Ophiolitic Massif, Cuba. *Spectrochimica Acta Part A: Molecular and Biomolecular Spectroscopy* 61, 1721–1728.
- Rinaudo, C., Gastaldi, D., Belluso, E., 2003. Characterization of chrysotile, antigorite and lizardite by FT-Raman spectroscopy. *The Canadian Mineralogist* 41, 883-890.
- Sack, R.O., Ghiorso, M.S., 1991. Chromian spinels as petrogenetic indicators: Thermodynamics and petrological applications. *American Mineralogist* 76, 827–847.
- Shen, P., Hwang, S.L., Chu, H.T., Jeng, R.C. 1988. STEM study of “ferritchromit” from the Heng-Chun chromitite. *American Mineralogist* 73, 383–388.
- Song S.G., Niu, Y.L., Zhang, L.F., Bucher, K., 2009. The Luliangshan garnet peridotite massif of the North Qaidam UHPM belt, NW China – a review of its origin and metamorphic evolution. *Journal of Metamorphic Geology* 27, 621–638.
- Stern, R.J., 2004. Subduction initiation: spontaneous and induced. *Earth and Planetary Science Letters* 226, 275–292.
- Stern, R.J., Gwinn, C.J., 1990. Origin of late Precambrian intrusive carbonates, Eastern Desert of Egypt and Sudan: C, O, and Sr isotopic evidence. *Precambrian Research* 46, 259–272.
- Stern, R.J., Johnson, P.R., Kröner, A., Yibas, B., 2004. Neoproterozoic ophiolites of the Arabian–Nubian Shield. In: Kusky, T.M. (Ed.), *Precambrian Ophiolites and Related Rocks: Development of Precambrian Geology* 13, 95–128.
- Streckeisen, A., 1976. Classification of common igneous rocks by mean of their chemical composition. A provisional attempt. *Neues Jahrbuch für Mineralogie – Abhandlungen* 1–15.
- Wang, A., Jolliff, B.L., and Haskin, L.A., 1999. Raman spectroscopic characterization of a Martian SNC meteorite: Zagami. *Journal of Geophysical Research*, 104, 8509–8519.
- Wang, A., Haskin, L.A., Kuebler, K.E., Jolliff, B.L., Walsh M.M., 2001. Raman spectroscopic detection of graphitic carbon of biogenic parentage in an ancient South African chert. Abstract No. 1423, *Lunar and Planetary Science XXXII*, Lunar and Planetary Institute, Houston, Texas.
- Wang, A., Freeman, J., and Kuebler, K.E. (2002) Raman Spectroscopic Characterization of Phyllosilicates. Abstract No.1374, *Lunar and Planetary Science XXXIII*, Lunar and Planetary Institute, Houston, Texas.
- Wang, A., Kuebler, K.E., Jolliff, B.L., Haskin, L.A., 2004. Raman spectroscopy of Fe-Ti-Cr-oxides, case study: Martian meteorite EETA79001. *American Mineralogist* 89, 665 – 680.
- Wiewióra, A., 1990. Crystallochemical classifications of phyllosilicates based on the unified system of projection of chemical compositions. *Clay Minerals* 25, 83–92.
- Wilson, M., 1989. *Igneous petrogenesis*: London, U.K., Unwin Hyman, 466 pp.
- Xie, X., Byerly, G.R., Ferrell, R.E.Jr., 1997. Trioctahedral chlorite: crystal structure and rock composition constraints with implications to geothermometry. *Contributions to Mineralogy and Petrology* 126, 275-291.
- Zanetti, A., D’Antonio, M., Spadea, P., Raffone, N., Vannucci, R., Bruguier, O., 2006. Petrogenesis of mantle peridotites from the Izu-Bonin-Mariana (IBM) forearc. *Ophioliti* 31(2), 189-206.
- Zang, W., Fyfe, W.S., 1995. Chloritization of the hydrothermally altered bedrock at the Igarape Bahia gold deposit, Carajas, Brazil. *Mineralogica Deposita* 30, 30–38.
- Zimmer, M., Kröner, A., Jochum, K.P., Reischmann, T., Todt, W., 1995. The Gabal Gerf complex: a Precambrian N-MORB ophiolite in the Nubian Shield, NE Africa. *Chemical Geology* 123, 29–51.